ELSEVIER

Comparison and implications from strikingly different authigenic carbonates in a Nyegga complex pockmark, G11, Norwegian Sea

Adriano Mazzini [a,*], Henrik Svensen [a], Martin Hovland [b], Sverre Planke [a,c]

[a] *Physics of Geological Processes (PGP), University of Oslo, PO Box 1048, Blindern, Norway*
[b] *Statoil, 4035 Stavanger, Norway*
[c] *Volcanic Basin Petroleum Research (VBPR), Oslo Research Park, 0349 Oslo, Norway*

Abstract

Authigenic carbonates sampled in a complex pockmark (G11) from the Nyegga area, south western Vøring Basin, reveal strikingly different morphologies. A comparative study of macro and micro features of these neighbouring samples was approached in order to attempt a reconstruction of the pockmark dynamics. The carbonate morphologies include thin (~ 1 cm) platy carbonate crusts, blocky and massive carbonate ridges up to several metres in size, and irregularly shaped carbonate deposits consisting of interconnected tubular and uneven intervals displaying high porosity. Our observations indicate that three distinct mechanisms of fluid seepage and carbonate precipitation occurred within the pockmark. Petrography studies reveal that the samples contain three generations of predominantly aragonitic cements. In addition, zoned crystals with coexisting Mg-calcite and dolomite are abundant in one sample suggesting a trend of gradual increase of the sulphate concentrations in the pore fluids during carbonate precipitation. Isotope measurements on bulk carbonate cements show consistent values with $\delta^{13}C$ as low as $-52.1‰$, $\delta^{18}O$ as high as 6.4‰, and $^{87/86}Sr$ of 0.7092. Anaerobic oxidation of methane close to seafloor conditions can explain these isotope data. The carbonates have a common carbon source despite the differences in morphology. Methane probably originated from the dissolution of gas hydrates as supported from calculated ^{18}O enrichment in the pore fluids and the methanogenic carbon. We propose a model where the differences in bulk carbonate morphology are related to local sediment properties, depth of carbonate precipitation and the flow rate of the seeping fluids.
© 2006 Elsevier B.V. All rights reserved.

Keywords: hydrocarbon seepage; gas hydrates; pockmark; carbonates; Vøring Plateau

1. Introduction

The precipitation of authigenic carbonates at fluid seepage sites is a common phenomenon that can be triggered by the activity of a consortium of *archaea* and bacteria that oxidize methane close to the seafloor (e.g. Boetius et al., 2000) or that can occur due to chemical reactions (i.e. without microbial mediation). Such carbonate deposits reveal different morphologies depending on combined internal (seepage-related) and external (setting-related) factors. Internal factors include the composition

---

and the flux of the seeping fluids, and the type of biological ongoing activity. External factors are the geological setting of the seepage area, the characteristics of the sediment flushed by fluids and finally the ongoing local erosion. The various carbonate shapes observed comprise exposed and buried mineralised doughnuts and chimneys from centimetre to metre-scale (e.g. Kulm and Suess, 1990; Aiello et al., 2001; Diaz-del-Rio et al., 2003; Mazzini et al., 2003), cemented fluid conduits and veins (Clari and Martire, 2000), concretions and micro- and macro-slabs laterally extensive on mud volcano surfaces (Aloisi et al., 2000; Mazzini et al., 2004), cemented sedimentary layers (Hovland et al., 1985; Hovland and Judd, 1988), build-ups of chemical authigenic carbonate and calcareous skeletal debris of chemosymbiotic fauna, or so called chemoherms (Beauchamp and Savard, 1992; Aharon, 1994; Clari et al., 1994; Mazzini et al., 2005) typically found on the seafloor or at shallow depths below the sediment–water interface.

Recently, both industry and academic cruises (e.g. Training Through Research program, TTR) investigated the Norwegian Sea focussing on the north-eastern flank of the Storegga Slide. Results documented authigenic seep carbonates in pockmarks showing a range of different morphologies (Kenyon et al., 1999; Kenyon et al., 2001; Hovland et al., 2005). Their formation could be related to destabilizing gas hydrates (Hovland et al., 2005; Mazzini et al., 2005; Hovland and Svensen, 2006). However, the dynamics of these systems are poorly understood, both regarding pockmark formation (explosive versus effusive), source of methane (thermogenic versus biogenic), reason for overpressure (gas generation versus loading), and timescale for seeps (active versus extinct).

In this paper we focus on the complex pockmark, G11, where differing carbonates samples were collected (Hovland et al., 2005). The relationship between fluid flows, local sediment properties, and carbonate morphologies, are investigated by a detailed structural, geochemical and mineralogical study of the carbonates. The origin of the fluids and the possible evidence of gas hydrates dissociation will be discussed combining data already published with the new results obtained.

2. Methods

Two detailed surveys in 2003–2004 were completed in the Nyegga area (Fig. 1) focussing on the G11 pockmark ($\sim$ N 64° 40′ 2″, $\sim$ E 05° 17′ 32″) including geophysical mapping, sea floor imaging, and seabed sampling using a DeepOcean ROV 'HiRov6'-system (see Hovland et al., 2005 for details). Three different types of carbonate deposits were sampled with the ROV's grabber arms.

Thin sections of three carbonate samples (G11-A–C) were studied using both optical and electronic microscopes, including UV light, secondary electron and backscattered electron modes. Microprobe analysis (53 data points) of calcite, aragonite and dolomite was done with a CAMECA SX 100 electron microprobe. X-ray diffraction analyses were performed on bulk carbonate samples to determine the dominant carbonate phase.

One of the samples (G11-C) was imaged using a GE Lightspeed Ultra CT 99_OC0 spiral computed tomography scanner, with an 8 sensor system. The thickness of the scanned slices was 0.625 mm, and more than 500 scans were made throughout the sample.

Carbon, oxygen, and strontium isotopic analyses were completed on carbonate samples. Carbonate cements were ground and digested with a 0.1 ml 100% H_3PO_4 solution for two hours at 30.0 °C in a vacuumed environment. The released CO_2 was transferred to a Finnigan MAT DeltaXP isotope ratio mass spectrometer (IRMS), for determination of $\delta^{13}C$ and $\delta^{18}O$. The analyses were controlled by house standards of calcite and aragonite. Results are reported in ‰ relative to the PDB standard. The precision for $\delta^{13}C$ is ±0.1‰ and for $\delta^{18}O$ ±0.2‰. Bulk crushed samples (10–20 mg) were used for Sr isotope analysis. The isotopic composition of Sr was determined by thermal ionization mass spectrometry (TIMS) on a Finnigan MAT 261.

3. Geological setting

The Nyegga region is located on the edge of the Norwegian continental slope (Fig. 1) on the border between two large sedimentary basins: the Møre Basin to the south and the Vøring Basin to the north (Brekke, 2000; Bünz et al., 2003). This region developed as a result of several rifting episodes leading to Late Paleocene/Early Eocene continental break-up and thermal subsidence (Skogseid and Eldholm, 1989; Brekke, 2000). Several dome-shaped structures, representing contraction structures of Late Eocene and Mid Miocene age, occur on this margin and are known to be potential traps for hydrocarbon reservoirs, such as the Ormen Lange dome south of Nyegga (Dore and Lundin, 1996; Vågnes et al., 1998). The seafloor of the Nyegga region is generally smooth, and consists of Plio–Pleistocene contourites and glacial–interglacial silty/clayey hemipelagic sediments of the Naust Formation which are acoustically parallel layered (Stuevold and Eldholm, 1996; Hjelstuen et al., 1999), covering the Miocene–Pliocene Kai Formation consisting of hemipelagic oozes faulted by polygonal systems (Rokoengen et al., 1995; Bünz et al., 2003). To the south, the giant retrogressive submarine Storegga
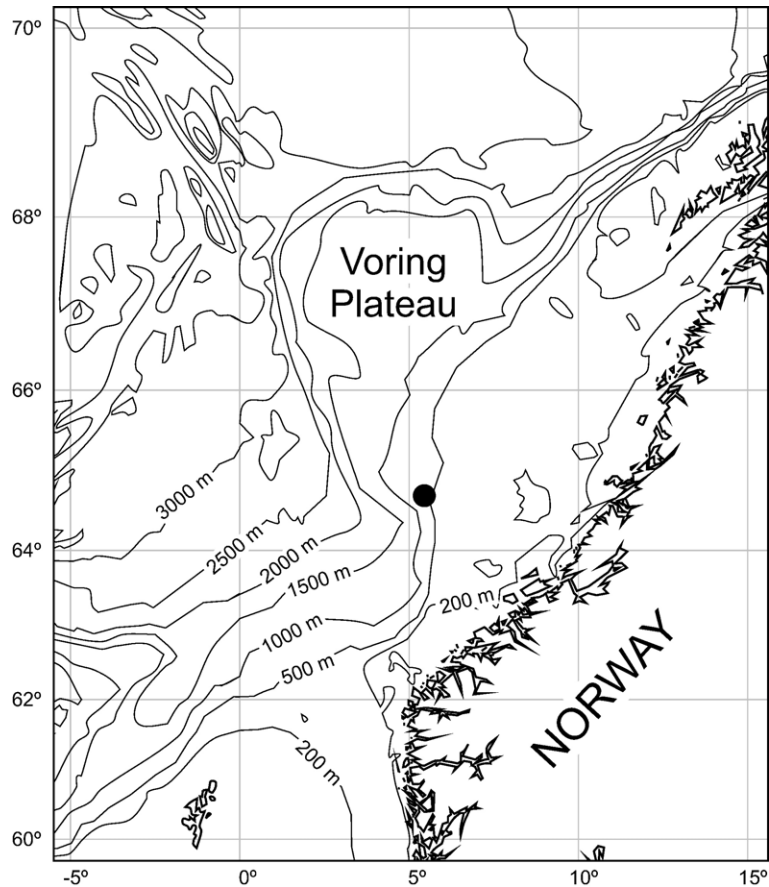
Fig. 1. Bathymetry of the mid-Norwegian margin. The position of pockmark G11 is indicated by a black dot.

Slide is the last of a series of slide events coupled to Pleistocene climatic fluctuations (Bugge et al., 1987; Mienert et al., 1998; Haflidason et al., 2003).

Fluid escape features like pockmarks and pipes are abundant in the Nyegga region (Bünz et al., 2003; Gravdal et al., 2003; Hovland et al., 2005). Furthermore, seismic studies show that the pockmarks are associated with a prominent bottom simulating reflector (BSR) that spreads to the north, west, and south of our study area (Mienert et al., 1998; Bouriak et al., 2000; Bünz et al., 2003). On 2D-seismic records, the pockmarks occur immediately above vertical 'chimneys' or pipes (also called 'wipeout'-zones, and 'blow-out pipes'), which extend down to and in some cases beyond the BSR (see Kenyon et al., 1999; Hovland et al., 2005). The source region of the pipes has been suggested to be both near the BSR and the Oligocene and Miocene polygonal fault horizons through which hydrocarbons supposedly seep from the domes sited below (Berndt et al., 2003; Bünz et al., 2003, 2005).

The studied pockmark G11 (Fig. 2) is located at about 730 m water depth in the Nyegga region. Its subrounded

shape is characterised by two irregular ridges separated by a central basin. The pockmark is about 260 m in diameter, is 11 m deep and contains small interior basins and 12 individual deposits of carbonate blocks some up to 24 m^3 in volume. The carbonate blocks and the surroundings are partly colonised by various fauna, including small tube-worms, stalked crinoids, ophiurids and sea spiders. Small patches of microbial mats were observed between some of the carbonate blocks (Hovland et al., 2005; Hovland and Svensen, 2006).
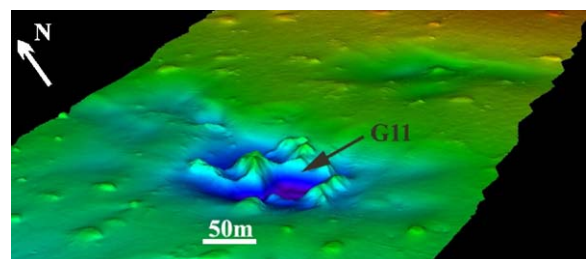

Fig. 2. High resolution bathymetry of the G11 pockmark.

4. Results

4.1. Macroscopic and petrography observations on carbonates

Although the sampling localities are situated only few tens of metres apart, striking morphological, structural and petrographic differences were observed among the three carbonate samples recovered (Table 1).

4.1.1. G11-A
G11-A was sampled from an area of the pockmark with flat hard substratum. A group of 0.5 m sized slabs was observed lying subhorizontally and partly covered by a thin veneer of hemipelagic sediment. The sample (Fig. 3A) is tabular and acicular crystals of aragonite cover the lower surface. The crust is characterized by finely spaced sub horizontal crystalline layers. The upper part is more massive with no visible porosity while the lower part is heterogeneous with more porous undulating layers (Fig. 3B).

Detailed petrography observations of sample G11-A reveal four main aragonite layers (Fig. 3B) with an internal structure characterised by several subparallel horizons of aragonite botryoids. Each layer is separated by darker irregular intervals with many voids that show higher content of Mg-calcite, pyrite and possibly organic remains at their base and top (intervals 1a, 2a, 3a). Partial oxidation to iron oxide is observed around pyrite framboids. Particularly interesting are the aragonitic intervals 1 and 4 consisting of uniform acicular aragonite characterised by a distinct layer rich in early zoned crystals of dolomite and Mg-calcite (Fig. 3C) in an aragonitic groundmass. The aragonite is fibrous and commonly zoned under ultra violet light (Fig. 3D).

4.1.2. G11-B
The G11-B sample is a fragment of a large massive carbonate block from a small ridge crossing the pockmark. The sample consists of homogeneous carbonate with some clayey sediment-filling cavities (Fig. 4A). The surface is dark grey, due to the presence of biofilm. The visible porosity is fairly low although some interconnected voids or cavities are present in the upper part of the sample.

Petrography reveals three compositional zones (Fig. 4B). The earliest cement in the central part of the sample consists of dark grey micritic aragonite binding together calcareous microfossils and siliciclastic material (mainly quartz, clay, and feldspar) (Fig. 4C). Besides the aragonite, the siliciclastic fraction is locally cemented by early micritic Mg-calcite. Pyrite framboids are observed throughout the micritic aragonite (Fig. 4D). A second generation of cement consists of light coloured botryoidal aragonite that forms rims around the darker first phase (Fig. 4B, E). A small amount of siliciclastic material and pyrite framboids are observed as aggregates between the large acicular crystals (Fig. 4F). The third type of cement consists of light-coloured fibrous aragonite that occurs as pore filling within the second generation, or as large crystal overgrowths on the external part of the sample.

4.1.3. G11-C
G11-C was sampled from an area with irregular seafloor adjacent to a pingo-like structure (Hovland and Svensen, 2006) colonized by various fauna and microbial mats. The sample consists of interconnected lobes and networks of carbonate cement with a very high porosity (Fig. 5A, B). Its structure is remarkably similar to coral deposits from reefs, although the main difference is the irregular sub-parallel zones with higher carbonate cement concentration. These irregular sub-horizontal layers are likely to indicate former sedimentary layering. The voids between the carbonate branches are circular or elliptical, varying from mm to cm scale. The sample was scanned with X-rays (CT Imaging) to image the internal structure and to evaluate the possible morphological effects of breaking off the carbonate during ROV sampling. Images taken through 0.6 mm scans show that the interior of the sample indeed resembles the exterior: the sample is composed of thin carbonate lobes connected by an irregular network of tubular features (Fig. 5B). An animated movie of the scans reveals the internal structure and the irregular distribution of the interconnected voids and the spherical pores. Irregularly shaped tubes (from

Table 1
Summary of samples described and main petrographic, morphological and geochemical characteristics

Sample	Shape	Carbonate minerals	$\delta^{18}O$ (‰PDB)	$\delta^{13}C$ (‰PDB)	$\delta^{13}C_{arag}$* (‰SMOW)	$\delta^{13}C_{Mg\ calc}$* (‰SMOW)
G11-A	Tabular	A+D+Mg	6.4	−52.1	1.6	2.3
G11-B	Blocky	A+Mg	5.6	−49.4	0.8	1.5
G11-C	Dendritic	A+Mg	5.2	−51.9	0.4	1.1

A = Aragonite, D = Dolomite, Mg = Mg calcite; $\delta^{13}C_{arag}$* = calculated $\delta^{18}O$ value of diagenetic fluids in isotopic equilibrium with aragonite at seafloor temperature around 0 °C; $\delta^{13}C_{Mg\ calc}$* = calculated $\delta^{18}O$ value of diagenetic fluids in isotopic equilibrium with Mg calcite at seafloor temperature around 0 °C; sea water composition at G11 location ~0.2‰$_{SMOW}$.
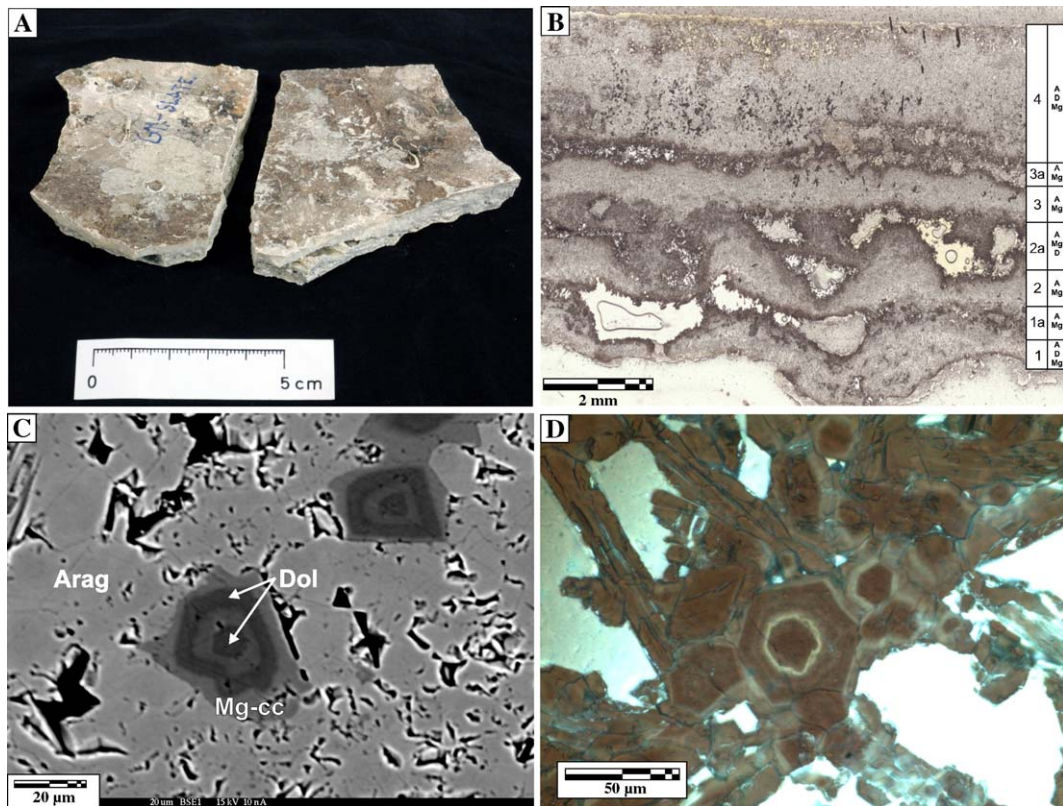
Fig. 3. Sample G11-A. (A) Tabular shaped hand specimen. The thickness of slabs varies between 7 and 10 mm. (B) Thin section image taken perpendicularly to lamination highlights the presence of subhorizontal aragonite-rich intervals (1, 2, 3, 4) separated by aragonite, Mg-calcite, pyrite, organic matter (?)-rich irregular intervals (1a, 2a, 3a). The upper part of interval 1a shows a transitional increase of pyrite framboids, siliciclastic admixture, and Mg-calcite crystals dispersed with a late diffusive aragonitic phase. This interval appears irregular on its upper and lower boundary where organic matter remains coat the aragonite crystals. Interval 2 consists of mainly aragonite crystals with some Mg-calcite. It is very similar to interval 1 except for the absence of zoned dolomite and Mg-calcite crystals. The upper part (2a) highlights enrichment of Mg-calcite and pyrite with occasional dolomite. Similarly to what observed for 1b, this interval shows distinct upper and lower boundaries with many voids in its central part. The last two distinct aragonite intervals with Mg-calcite (3–4) appear very similar to previously described intervals 1 and 2. They are also separated by a thin interval richer in Mg-calcite and pyrite that transitionally extends in the most recent aragonitic phase 4; carbonate mineral contents are indicated by A=Aragonite, D=Dolomite, Mg=Mg-calcite. (C) SEM backscatter mode image from interval 1 showing zoned crystals of dolomite and Mg-calcite in aragonitic groundmass. (D) Plane light and UV-light thin section image; in the centre of the image are visible sections of aragonite needles with different growth stages.

mm to cm size) are observed crossing through the sample with orientation mainly orthogonal to the parallel layering (Online Background Dataset).

Three main mineralogical textures were found. The first cementation phase appears in the central part of the lobes. It consists of micritic aragonite, and, in lesser amount, of early Mg-calcite cementing fine-grained siliciclastic material (mainly quartz, K-feldspar, and clay minerals) (Fig. 5C, E). A few plagioclase grains show evidence of dissolution and illite/smectite precipitation, possibly representing in situ alteration. Microfossils are abundant and are sometimes filled by aragonite crystals. Embayments and local voids present in this phase are locally filled with fibrous aragonite (Fig. 5D). The last aragonitic phase consists of large acicular botryoids that

appear to cover the sample and to grow within the vesicles and cavities. Two-phase fluid inclusions (few microns in size) are observed in the acicular aragonite crystals. Microbial biofilm is observed coating the last carbonate phase (Fig. 5F), similarly to that observed by Mazzini et al. (2005, Fig. 6a).

4.2. Carbonate geochemistry

Microprobe point analyses were conducted on the different cement generations and on all carbonate mineral phases in the three samples. Representative analyses are shown in Table 2 and all data points are plotted in Fig. 6. The dataset reveals no systematic variations in carbonate geochemistry between the early and late stage cements
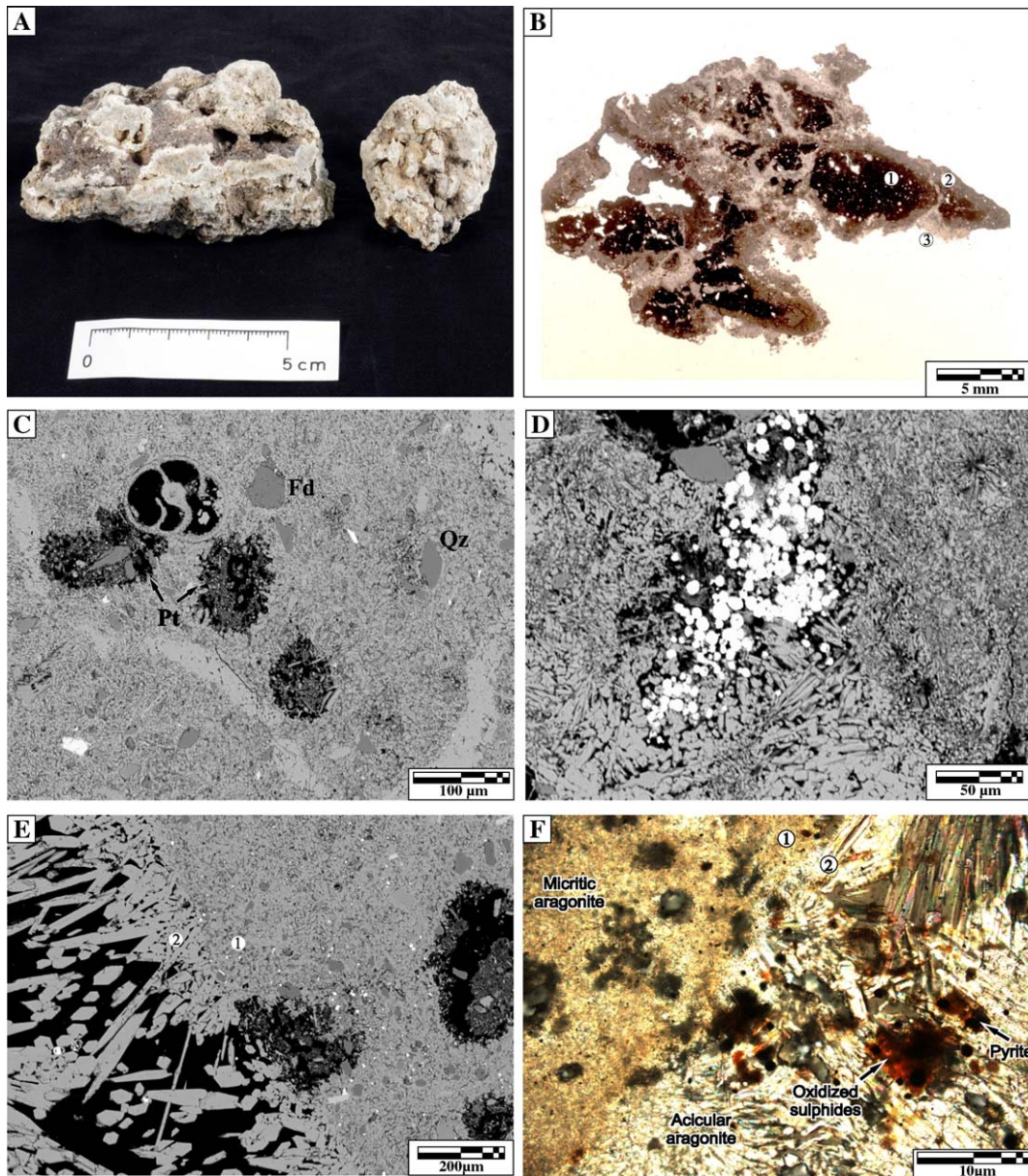
Fig. 4. Sample G11-B. (A) Fragment of the porous block. Note dark colour ascribed to microbial mat covering the external surface of the sample, the numerous cavities and zonations in the internal part of the sample. (B) Thin section image of the sample highlighting the different zones including (1) dark central part (aragonite + siliciclastic sediment), (2) lighter coloured rims (botryoidal aragonite) around dark zones and (3) whitish pore filling aragonite. (C) SEM backscatter image of zone 1; note the grey siliciclastic grains (Qz, Fd), the darker clayey pellets (Pt), and the microfossil (top left) within the micritic aragonite groundmass. (D) SEM backscatter image of zone 1 showing pyrite framboids (high backscatter in the central part of the image) within aragonitic cement. (E) SEM backscatter image of contact between micritic zone 1 (right side) and acicular zone 2 (left side). (F) Thin section image with contact between zone 1 (left side) and zone 2 (right side), note the pyrite framboids between the acicular crystals (dark coloured) and oxidation around the framboids.

within the each sample. The MgO content of the calcite in G11-A varies between 4.8 and 7.5 wt.%, whereas the content in G11-C shows lower values (2.5 wt.%). The Mg-calcite in G11-A recalculated to structural formulas corresponds to 12–20 mol% Mg. All the samples show aragonite with very low MgO concentrations (generally lower than 0.01 wt.%), FeO content is up to 0.5 wt.% whereas the MnO content is generally lower than 0.4 wt.%. The SrO concentrations in aragonite vary between 0 and 1.8 wt.%, with an average of 0.88 wt.%. The average Sr/Ca
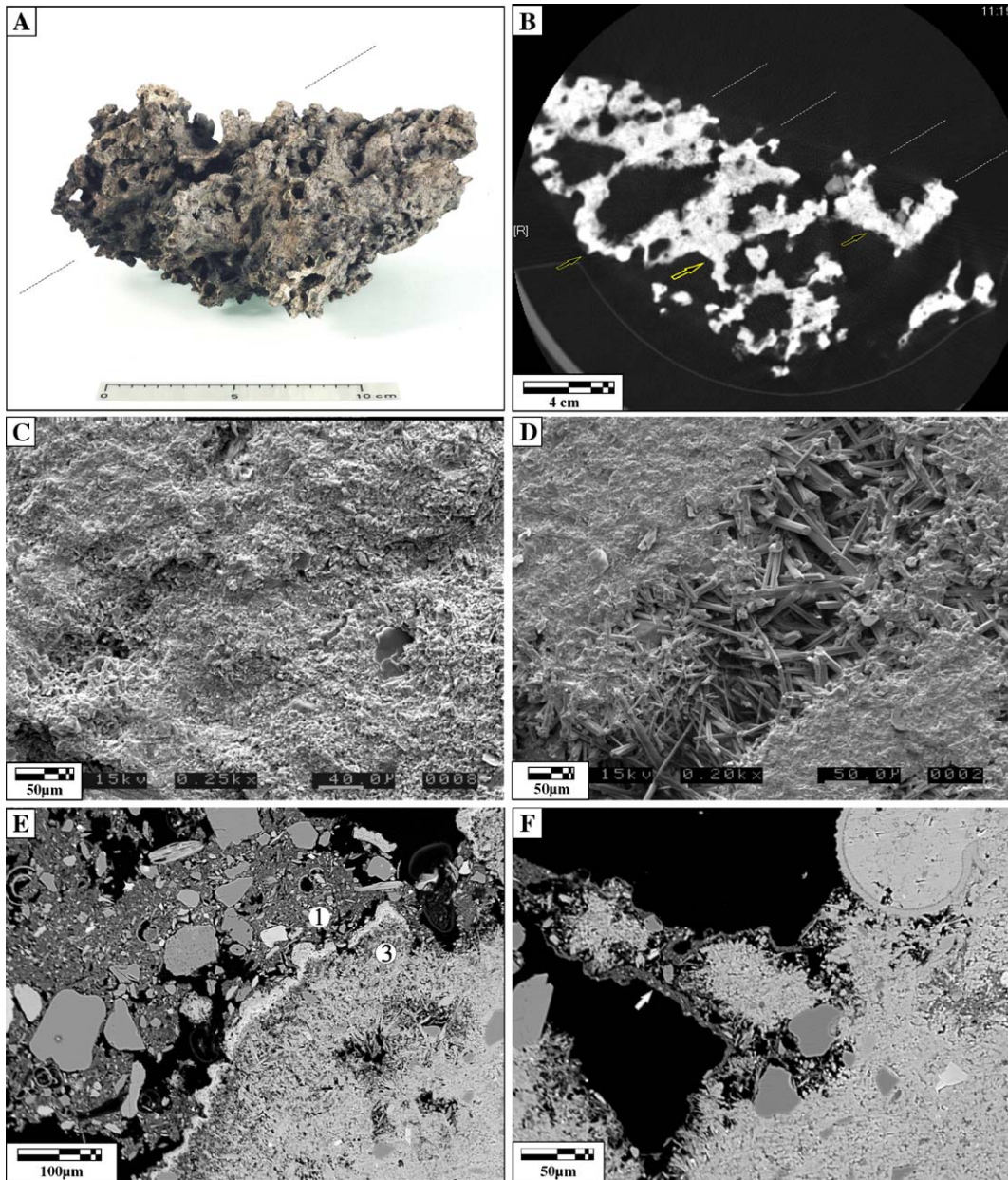
Fig. 5. Sample G11-C. (A) Sample fragment showing irregular shape and interconnected lobes, note the thicker layers within the sample (orientation NE–SW on dashed lines) that represent the original sedimentary layers. (B) CT Imaging slice showing the internal structure of the sample consisting of thicker subparallel carbonate layers (on dashed lines) interconnected by tubular features (white arrows). (C) SEM image of micritic aragonite groundmass. (D) SEM image of micritic aragonite and pore filling acicular aragonite (central part of the image). (E) SEM thin section backscatter image of siliciclast sediment-rich micritic aragonite (1, left) and coating acicular aragonite (3, right). (F) SEM thin section backscatter image showing detail of last aragonitic phase, note the microbial coating around the aragonite needles (arrowed).

molar ratio is 0.016, which is close to the marine water ratio (0.020). High Mg-calcite cement and foraminifera shells have the lowest calculated Sr content per formula unit (pfu). The Sr content in aragonite varies from 0.008 to 0.03 pfu, while the most Sr-enriched aragonites are from sample G11-A.

An outstanding feature of the G11-A sample is the single crystal zoning of Mg-calcite and dolomite. Microprobe analyses of the calcite and dolomite show 12–18 mol% MgO and 35–48 mol% MgO, respectively (Table 2). The Mg content between 0.7 and 0.8 pfu in many of the analyses suggests either some contamination
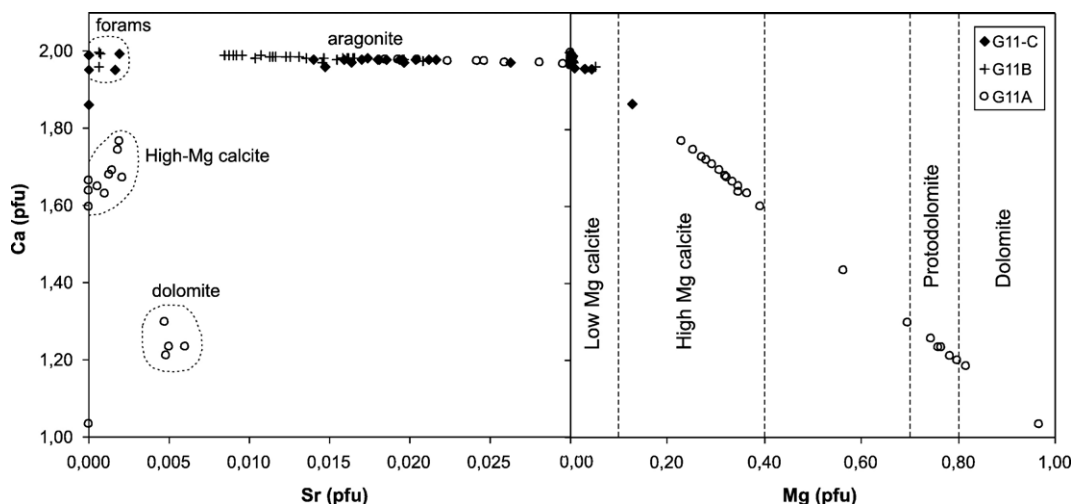
Fig. 6. Electron microprobe plot of Sr, Mg versus Ca in aragonite, calcite, and dolomite. Electron microprobe plot of Sr, Mg versus Ca. Calculation of standard formulas from the electron microprobe analysis shows that the various carbonates differ in Sr content. High Mg- calcite and foraminifera shells have the lowest Sr content per formula unit (pfu). The Sr content in aragonite varies from 0.008 to 0.03 pfu, while the most Sr-enriched aragonites are from sample G11-A. The dolomite shows a Sr concentration between that of calcite and aragonite. The Mg content between 0.7 and 0.8 pfu in many of the analyses suggests either some contamination of calcite during microprobe analysis, or that most of the crystals are protodolomite.

of calcite during microprobe analysis, or that most of the crystals are protodolomite. Up to five zones with alternating Mg-calcite and dolomite are observed. The strontium content is consistently higher in the dolomite than in the Mg-calcite, and always higher in the aragonite surrounding the crystals.

4.3. Isotopes

Strontium stable isotope analyses were completed on sample G11-C. Data reveal that the bulk $^{87/86}$Sr is 0.709168 (+/−0.000018). This is similar to the present-day composition of seawater of 0.7091 (Jones and Jenkyns, 2001).

The bulk δ^{13}C and δ^{18}O isotopic composition of the three samples (Table 1) shows relatively strong ^{13}C depletion (δ^{13}C as low as −52.1‰) and moderately high δ^{18}O values (from 5.2‰ to 6.4‰). Similar values were recorded by Mazzini et al. (2005) from chemoherms from a pockmark located in the same region (Fig. 7).

5. Discussion

5.1. Methane fuelling carbonate precipitation

The ^{13}C depletion recorded from the carbonates indicates that the carbon derived from the anaerobic oxidation of methane (AOM) resulting in an increase in pore fluid bicarbonate and thus carbonate precipitation (e.g. Hovland et al., 1985; Ritger et al., 1987; Boetius et al., 2000). The reaction of sulphate reduction, usually coupling the AOM at seepage locations, is suggested by

the presence of pyrite in the carbonate samples (Hovland et al., 1987; Beauchamp and Savard, 1992; Mazzini et al., 2004). This confirms that the carbonates formed during shallow burial in the sulphate reduction zone.

Interestingly, methane carbon isotope measurements from the G11 pockmark shows values as low as −69‰ (Hovland et al., 2005) revealing a depletion almost 20‰ higher than the related carbonates. The possibility of some contamination of heavier carbon (e.g. from sedimentary matrix, coccoliths and or small foraminifera) in the carbonate cannot be disregarded, nevertheless the difference in depletion between methane and authigenic carbonate is similar to that observed by Mazzini et al. (2004) in the Black Sea. This supports the idea that transportation processes and kinetic fractionation of methane can be responsible for the shift in ^{13}C depletion.

The controversial and debated origin of the methane fuelling the carbonate precipitation can be defined combining the results from this study with the ones already published. It appears that the carbonates recorded a mixture of partly thermogenic/biogenic methane. Deep rooted pipes below pockmarks are assumed to be pathways for thermogenic methane located at greater depth later forming gas hydrates (Posewang and Mienert, 1999; Andreassen et al., 2000). The presence of a thermogenic gas component at the seafloor was furthermore described by Mazzini et al. (2005) and by Hovland et al. (2005). Hydrocarbons of different chain lengths (C1–C5) were recorded within the carbonate–cement fluid inclusions, and in the free gas respectively. Nevertheless methane and carbonate δ^{13}C values indicate a significant input from

Table 2
Selected electron microprobe analysis of carbonates (wt.% oxides) and calculated structural formulae

| Sample	G11-A							G11-B				G11-C					
Mineral	Mg-cc	dol	arag	dol	Mg-cc	Mg-cc	arag	arag	arag	arag	foram	Mg-cc	arag	arag	arag	arag	foram
MgO	4.82	16.57	0.00	16.19	6.63	6.87	0.00	0.00	0.00	0.00	0.01	2.51	0.00	0.00	0.00	0.00	0.87
CaO	52.09	35.72	54.82	36.53	48.64	45.09	54.23	53.03	55.35	55.03	55.90	50.29	54.43	54.60	53.13	54.89	53.22
MnO	0.02	0.03	0.10	0.00	0.01	0.03	0.02	0.01	0.04	0.00	0.01	0.02	0.02	0.00	0.01	0.04	0.01
FeO	0.03	0.02	0.00	0.00	0.02	0.50	0.02	0.16	0.03	0.03	0.03	0.26	0.00	0.05	0.11	0.06	0.08
SrO	0.10	0.26	0.94	0.33	0.07	0.00	1.83	1.03	0.47	0.84	0.03	0.00	1.34	0.95	0.89	0.87	0.08
Total	57.06	52.60	55.86	53.05	55.36	52.48	56.08	54.23	55.86	55.91	55.98	53.08	55.79	55.60	54.15	55.87	54.27
Structural formulae based on 2 cations (mole per formula unit)																	
Mg	0.228	0.782	0.000	0.761	0.319	0.347	0.000	0.000	0.000	0.000	0.001	0.129	0.000	0.000	0.000	0.000	0.001
Ca	1.769	1.212	1.979	1.234	1.679	1.638	1.964	1.974	1.990	1.983	1.998	1.863	1.973	1.980	1.978	1.980	1.998
Mn	0.000	0.001	0.003	0.000	0.000	0.001	0.000	0.000	0.001	0.000	0.000	0.001	0.000	0.000	0.000	0.001	0.000
Fe	0.001	0.000	0.000	0.000	0.001	0.014	0.001	0.005	0.000	0.001	0.001	0.007	0.001	0.002	0.003	0.002	0.001
Sr	0.002	0.005	0.018	0.006	0.001	0.000	0.036	0.021	0.009	0.016	0.001	0.000	0.026	0.019	0.018	0.017	0.001
Mol% Mg	11.4	39.2	0.0	38.1	16.0	17.4	0.0	0.0	0.0	0.0	0.1	6.5	0.0	0.0	0.0	0.0	0.1
Sr/Ca molar	0.001	0.004	0.009	0.005	0.001	0.000	0.018	0.011	0.005	0.008	0.001	0.000	0.013	0.009	0.009	0.009	0.001
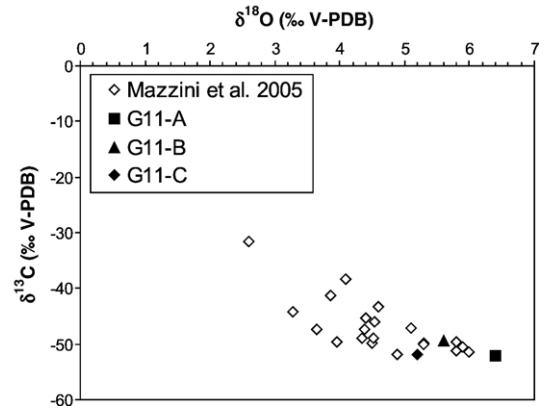
Fig. 7. Cross-plot of carbon ($\delta^{13}C$) and oxygen ($\delta^{18}O$) stable isotope compositions for carbonate cements.

biogenic methane. Thus there is mixing with biogenic methane generated at shallow depth (Kvenvolden et al., 1989; Whiticar and Faber, 1989; Mazzini et al., 2005) that could be incorporated in the shallow gas hydrates.

5.2. Gas hydrates in the near subsurface?

As described in the Introduction, the presence of gas hydrates in the region has been inferred by numerous authors (e.g. Hovland and Svensen, 2006); nevertheless hitherto no direct evidence of hydrates has been documented. Only during a recent marine expedition (Training Through Research Cruise, TTR16) gas hydrates were finally sampled from this area and further analyses are currently being undertaken. In the following section former and new evidences supporting the presence of gas hydrates will be given.

The water depth (738–723 m) and the temperature (~0 °C) recorded at the G11 pockmark indicate that the location lies within the gas hydrates stability field up to 200 m below the seafloor (Mienert and Posewang, 1999; Posewang and Mienert, 1999). Furthermore, several authors have documented BSR on seismic data (e.g. Bouriak et al., 2000; Bünz et al., 2003; Hovland et al., 2005). Possible dissociation of gas hydrates at G11 is also recorded in the authigenic carbonates. The aragonite analysed is strontium-rich in all samples, which is common in settings where aragonite is interpreted to have precipitated from sea water (e.g. Savard et al., 1996; Peckmann et al., 2001). This suggests that the Sr was derived from seawater or from pore fluids not significantly affected by fluid–rock interaction (i.e., early-diagenetic pore waters). This is also confirmed by both the molar Sr/Ca ratios and the Sr isotopes of the aragonites. Taken this into account, the estimations of the $\delta^{18}O$ values of diagenetic fluids in isotopic equilibrium with Mg calcite

and aragonite at seafloor temperature have been calculated applying respectively the Friedman and O'Neil (1977) Grossman and Ku (1986) equation (Table 1). These values are greater than the 0.2‰$_{SMOW}$, present value of Nyegga region bottom water (Tchernia, 1978), indicating that the cements precipitated from a fluid enriched in ^{18}O. Fluids released from the dissolution of gas hydrates could explain these values; nevertheless it is difficult to rule out other alternatives such as clay mineral dehydration. Support for local gas hydrate dissociation is also given by the specific regional oceanography, where the seasonal and decadal depth variation of the thermocline could influence the

stability of underlying sediment-hosted gas hydrates (Mork and Blindheim, 2000; Orvik and Skagseth, 2003; Hovland et al., 2005). However a warming of 7–10 °C is estimated to be needed at this location in order to dissociate gas hydrates (cf. Dickens et al., 1997).

5.3. Geochemical control of the mineralogy

The carbonate generations observed in the samples demonstrate an initial phase of dolomite and Mg-calcite precipitation followed by at least three stages of precipitation of micritic and acicular aragonite. The inhibition of
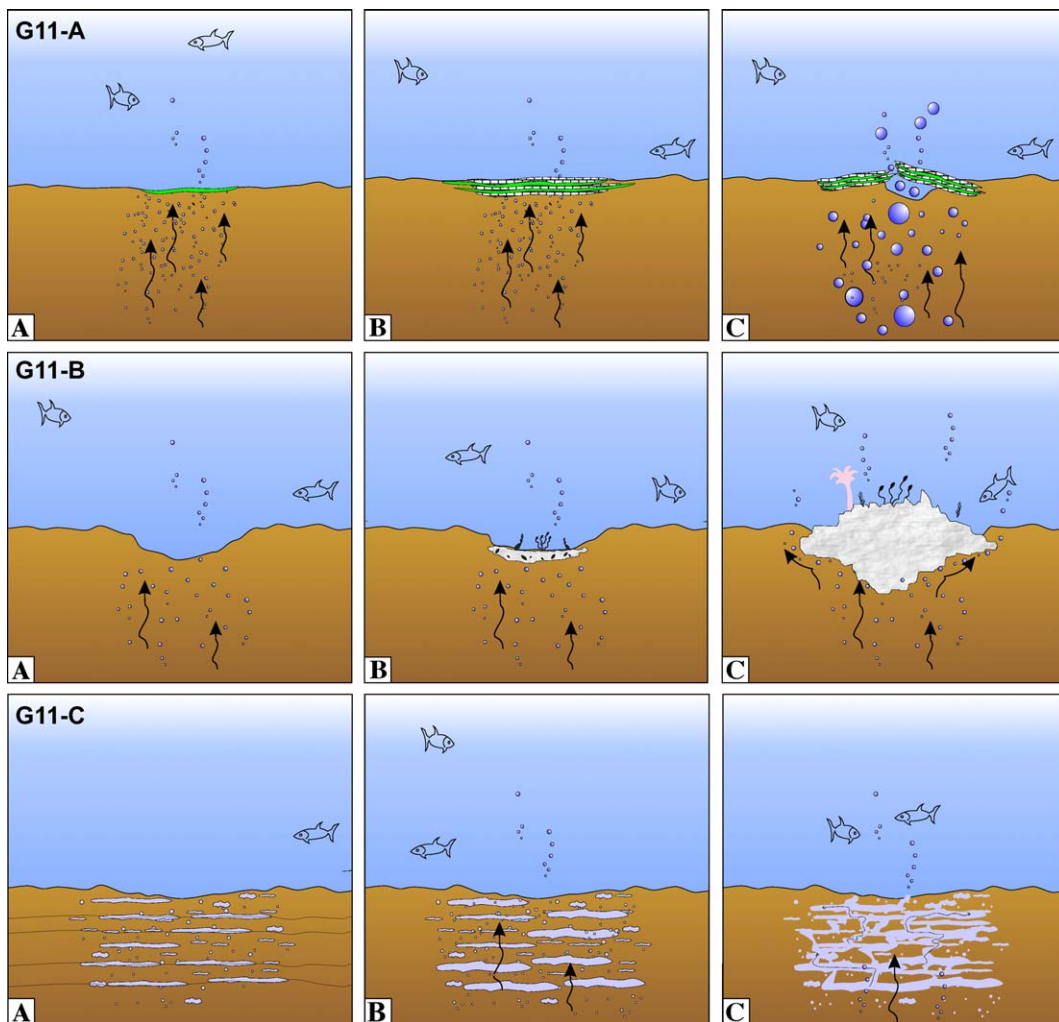

Fig. 8. Schematic evolutionary model of carbonate formation. G11-A: (A) slow hydrocarbon seepage on smooth seafloor where microbial mats concentrate at seepage site initiating AOM; (B) precipitation of authigenic carbonate on the seafloor forming laterally extensive slabs; microbial mats are separated by aragonite rich layers; (C) sustained seepage and burst of large gas pockets that were expelled on the seafloor breaking through the carbonate slabs. G11-B: (A) diffused hydrocarbon seepage and formation of pockmarks on the seafloor; (B) precipitation of authigenic carbonate on the near subsurface; (C) formation of large carbonate deposits that impede the vertical seepage of fluids deviating it laterally enhancing lateral growth. G11-C: (A) gas hydrates aggregates concentrated at the interface between the sedimentary layers; (B) volume increase due to dissolution of the gas hydrates and beginning of seepage; (C) fluids preferentially seep vertically along tubular features and more diffusely horizontally along former gas hydrate layers.

calcite precipitation versus aragonite in sulphate-rich dia-genetic environments has been described by several authors (e.g. Naehr et al., 2000; Aloisi et al., 2002). The evolution from dolomite, micritic calcite to aragonite (Fig. 3C) observed in the Nyegga samples could indicate precipitation at different depths below the seafloor as-suming a gradual decrease of sulphates with depth (e.g. Mazzini et al., 2005).

However, this ultimately depends on fluid composi-tion (e.g. Burton, 1993). For instance, an increase in porewater sulphate (e.g. due to a gradual decrease in seepage allowing sulphate-rich fluids to move in the close subsurface, or due to partial erosion) could favour aragonite over Mg-calcite or dolomite.

5.4. Implications for carbonate precipitation dynamics and mineralogical phases

Following the "freeze–thaw" model of Krause (2001), Hovland et al. (2005) suggested a generic model of slow dissociation of gas hydrates in the subsurface. With a more complex model also involving an abrupt release of trapped gases, the authors described the general formation model of the pockmarks in the Nyegga area. We propose three simplified qualitative and conceptual models to describe the precipitation of different types of carbonate deposits present in the G11 pockmark.

The horizontal subparallel mineralogical layering observed on sample G11-A suggests that carbonate pre-cipitated very close to the seafloor during slow hydrocar-bon seepage. We suggest that microbial colonies of e.g. *Beggiatoa* thriving at the seafloor may have generated anoxic conditions in the immediate subsurface. In this anoxic environment various other microbial colonies grew, thus forming defined layers allowing the precipi-tation of carbonates in between (Fig. 8). This hypothesis is supported by the absence of siliciclastic sediment and by the presence of three different carbonate phases ascribed to the AOM occurring in the top few centimetres of the seafloor. The pyrite- organic- Mg-calcite-rich layers (i.e. 1a, 2a, 3a, Fig. 3B) are interpreted as microbial layers where consortia of sulphate reducing bacteria and meth-ane oxidizing *archaea* were concentrated enhancing cyclic subparallel carbonate precipitation.

The elongated carbonate ridge sampled at location G11-B suggests that hydrocarbon-rich fluids were seeping in the pore media along preferential pathways (e.g. fractures) inducing significant precipitation of authigenic carbon-ate around the detrital grains. The last aragonitic phases (phases 2–3) are devoid of siliciclastic sediment suggest-ing that no sedimentary capping was present at the moment of precipitation. Similarly to G11-A sample, the dark grey microbial coating (*Beggiatoa*?) on the external part could have caused anoxic conditions immediately below, thus allowing the precipitation of aragonite via AOM.

This type of deposits is now found outcropping as high build-ups and ridges (Fig. 8) likely due to erosion of the fine grained sediment thus exhuming the carbonates. The gradual collapse of the structure is demonstrated by large blocks nearby the ridges. These carbonate blocks rest on the clay-rich sediment fill in the pockmark, but they are usually not covered by clay, suggesting active erosion.

The unusual structure of sample G11-C suggests a more dynamic formation mechanism. Changes in pressure and temperature conditions presumably triggered the gas hydrates dissociation in the near subsurface resulting in volume increase and enhancing the seepage of fluids through preferential pathways (e.g. microfractures, sedi-ment unconformities, bioturbation burrows). The layering and the irregularly oriented tubular features observed in the hand specimen suggest that: (a) the methane-rich fluids seepage concentrated in the tubular channels; (b) diffusive flow occurred horizontally where the volume previously occupied by gas hydrates was replaced by carbonate cement. The progressive cementation of the tubular features and the subhorizontal voids can explain the dendritic irregular shape characterizing this sample (Fig. 8). The presence of porous cm sized carbonate vesicles could also be explained assuming that the sample represents an imprint of gas hydrates. Such features have been observed also on gas hydrate deposits, e.g. in the Cascadia margin, by several authors (e.g. Bohrmann et al., 1998; Suess et al., 2002; Teichert et al., 2005). Moreover, tomography analyses on these porous clathrates showed the presence of cm sized free gas bubbles incorporated within the crystals (Abegg et al., 2002). It is suggested that the vesicles and the subrounded features described in carbonate sample G11-C, represent portions of free gas originally present in the hydrates. Like in the model suggested for sample G11-B, erosion operated by currents is expected to have exposed the carbonate structure on the sea floor.

6. Conclusions

Unique sampling in the G11 pockmark allowed the comparison of authigenic carbonates with contrasting morphologies. We conclude that:

- Microbial oxidation of methane triggered the pre-cipitation of three carbonate generations within the pockmark.
- The mineralogical association of dolomite, Mg-calcite and aragonite is interpreted as due to local variation in the porewater sulphate content that probably occurred

during partial erosion, exhumation, or during a temporary decrease in seep activity.

- The bulk isotope composition of the samples suggests precipitation from the same type of pore fluid. Oxygen isotopes reveal anomalous ^{18}O enrichment compared with normal seawater pore fluids, pointing towards a gas hydrate origin.
- A gas hydrate origin is supported by a network-like morphology of the volumetrically dominant carbonate rock type.
- High Sr concentrations in aragonite suggests a Sr and cation source from seawater or shallow pore fluids.
- The remarkable morphological differences of the samples reflect contrasting settings and mechanisms of precipitation (i.e. seafloor precipitation during slow diffusive flow, G11-A; microseepage of gas in the pore media, G11-B; more sustained seepage in the subsurface ascribed to gas hydrate dissociation; G11-C).

Acknowledgements

Appendix A. Supplementary data

Supplementary data associated with this article can be found, in the online version, at doi:10.1016/j.margeo.2006.05.012.

References

Abegg, F., Bohrmann, G., Freitag, J., Kipfstuhl, S., 2002. Structure and distribution of gas hydrates in marine sediments, 7th International Conference "Gas in marine sediments", Baku, Azerbaijan, pp. 5–7.

Aharon, P., 1994. Geology and biology of modern and ancient submarine hydrocarbon seeps and vents: an introduction. Geo Mar. Lett. 14, 69–73.

Aiello, I.W., Garrison, R.E., Moore, J.C., Kastner, M., Stakes, D.S., 2001. Anatomy and origin of carbonate structures in a Miocene cold-seep field. Geology 29 (12), 1111–1114.

Aloisi, G., Pierre, C., Rouchy, J.M., Foucher, J.P., Woodside, J., 2000. Methane-related authigenic carbonates of eastern Mediterranean Sea mud volcanoes and their possible relation to gas hydrate destabilisation. Earth Planet. Sci. Lett. 184 (1), 321–338.

Aloisi, G., Bouloubassi, I., Heijs, S.K., Pancost, R.D., Pierre, C., Sinninghe Damste, J.S., Gottschal, J.C., Forney, L.J., Rouchy, J.-M.,

2002. CH_4-consuming microorganisms and the formation of carbonate crusts at cold seeps. Earth Planet. Sci. Lett. 203 (1), 195–203.

Andreassen, K., Mienert, J., Bryn, P., Singh, A., 2000. A double gas-hydrate related bottom simulating reflector at the Norwegian continental margin. Ann. N.Y. Acad. Sci. 912, 126–135.

Beauchamp, B., Savard, M., 1992. Cretaceous chemosynthetic carbonate mounds in the Canadian Arctic. Palaios 7 (4), 434–450.

Berndt, C., Bunz, S., Mienert, J., 2003. Polygonal fault systems on the mid-Norwegian margin: a long-term source for fluid flow. In: Van Rensbergen, P., Hillis, R.R., Maltman, A.J., Morley, C.K. (Eds.), Subsurface Sediment Mobilization. Special Publication — Geological Society of London. Geological Society, pp. 283–290.

Boetius, A., Ravenschlag, K., Schubert, C.J., Rickert, D., Widdel, F., Gieseke, A., Amann, R., Jorgensen, B.B., Witte, U., Pfannkuche, O., 2000. A marine microbial consortium apparently mediating anaerobic oxidation of methane. Nature 407, 623–625.

Bohrmann, G., Greinert, J., Suess, E., Torres, M., 1998. Authigenic carbonates from the Cascadia subduction zone and their relation to gas hydrate stability. Geology 7, 647–650.

Bouriak, S., Vanneste, M., Saoutkine, A., 2000. Inferred gas hydrates and clay diapirs near the Storegga Slide on the southern edge of the Vøring Plateau, offshore Norway. Mar. Geol. 163 (1–4), 125–148.

Brekke, H., 2000. The tectonic evolution of the Norwegian Sea continental margin, with emphasis on the Voring and More basins. In: Nottvedt, A. (Ed.), Dynamics of the Norwegian Margin. Special Publication — Geological Society of London. Geological Society, pp. 327–378.

Bugge, T., Befring, S., Belderson, R.H., Eidvin, T., Jansen, E., Kenyon, N., Holtedahl, H., Sejrup, H.P., 1987. A giant three-stage submarine slide off Norway. Geo Mar. Lett. 7, 191–198.

Bünz, S., Mienert, J., Berndt, C., 2003. Geological controls on the Storegga gas-hydrate system of the mid-Norwegian continental margin. Earth Planet. Sci. Lett. 209 (3–4), 291–307.

Bünz, S., Mienert, J., Bryn, P., Berg, K., 2005. Fluid flow impact on slope failure from 3D seismic data: a case study in the Storegga Slide. Basin Res. 17 (1), 109–122.

Burton, E.A., 1993. Controls on marine carbonate cement mineralogy: review and reassessment. Chem. Geol. 105 (1/3), 163.

Clari, P., Fornara, L., Ricci, B., Zuppi, G.M., 1994. Methane-derived carbonates and chemosymbiotic communities of Piedmont (Miocene, northern Italy). Geo Mar. Lett. 14, 201–209.

Clari, P., Martire, L., 2000. Cold seep carbonates in the Tertiary of northwest Italy: evidence of bacterial degradation of methane. In: Riding, R.E., Awramik, S.M. (Eds.), Microbial Sediments. Springer-Verlag, Berlin, Heidelberg, pp. 261–269.

Diaz-del-Rio, V., Somoza, L., Martinez-Frias, J., Mata, M.P., Delgado, A., Hernandez-Molina, F.J., Lunar, R., Martin-Rubi, J.A., Maestro, A., Fernandez-Puga, M.C., 2003. Vast fields of hydrocarbon-derived carbonate chimneys related to the accretionary wedge/olistostrome of the Gulf of Cadiz. Mar. Geol. 195 (1–4), 177–200.

Dickens, G.R., Castillo, M.M., Walker, J.C.G., 1997. A blast of gas in the latest Paleocene: simulating first-order effects of massive dissociation on oceanic methane hydrate. Geology 25 (3), 259–262.

Dore, A.G., Lundin, E.R., 1996. Cenozoic compressional structures on the NE Atlantic margin: nature, origin and potential significance for hydrocarbon exploration. Petrol. Geosci. 2 (4), 299–311.

Friedman, I., O'Neil, J.R., 1977. Compilation of stable isotope fractionation factors of geochemical interest, In: Fleisher, M. (Ed.), Data of Geochemistry, 6th ed. USGS Prof. Paper, p. 12.

Gravdal, A., Haflidason, H., Evans, D., 2003. Seabed and subsurface features on the southern Vøring Plateau and northern Storegga

slide escarpment. In: Mienert, J., Weaver, P. (Eds.), European Margin Sediment Dynamics. Springer, Berlin, pp. 111–117.

Grossman, E.L., Ku, T.L., 1986. Carbon and oxygen isotope fractionation in biogenic aragonite: temperature effects. Chem. Geol. 59, 59–74.

Haflidason, H., Sejrup, H.P., Berstad, I.M., Nygård, A., Richter, T., Bryn, P., Lien, R., Berg, K., 2003. A weak layer feature on the northern Storegga Slide Escarpment. In: Mienert, J., Weaver, P. (Eds.), European Margin Sediment Dynamics. Springer, Berlin, pp. 55–62.

Hjelstuen, B.O., Eldholm, O., Skogseid, J., 1999. Cenozoic evolution of the northern Voring margin. Bull. Geol. Soc. Am. 111 (12), 1792–1807.

Hovland, M., Judd, A.G., 1988. Seabed pockmarks and seepages: impact on geology, biology and the marine environment. Graham & Trotman, p. 293.

Hovland, M., Svenson, H., 2006. Submarine pingoes: indicators of shallow gas hydrates in a pockmark at Nyegga, Norwegian Sea. Mar. Geol. 228, 15–23.

Hovland, M., Talbot, M.R., Olaussen, S., Aasberg, L., 1985. Recently formed methane-derived carbonates from the North Sea floor. In: Thomas, B.M. (Ed.), Petroleum Geochemistry in Exploration of the Norwegian Shelf. Norwegian Petroleum Soc. Graham & Trotman, pp. 263–266.

Hovland, M., Talbot, M.R., Qvale, H., Olaussen, S., Aasberg, L., 1987. Methane-related carbonate cements in pockmarks of the North Sea. J. Sediment. Petrol. 57 (5), 881–892.

Hovland, M., Svensen, H., Forsberg, C.F., Johansen, H., Fichler, C., Fossa, J.H., Jonsson, R., Rueslatten, H., 2005. Complex pockmarks with carbonate-ridges off mid-Norway: products of sediment degassing. Mar. Geol. 218 (1–4), 191–206.

Kenyon, N.H., Ivanov, M.K., Akhmetzhanov, A.M. (Eds.), 1999. Geological Processes on the Northeast Atlantic Margin. Technical Series — Intergovernmental Oceanographic Commission, vol. 54, p. 141.

Kenyon, N.H., Ivanov, M.K., Akhmetzhanov, A.M., Akhmanov, G.G. (Eds.), 2001. Multidisciplinary Study of Geological Processes on the North East Atlantic Margin and Mid-Atlantic ridge. Technical Series — Intergovernmental Oceanographic Commission, vol. 60, p. 142.

Krause, F.F., 2001. Genesis and geometry of the Meiklejohn Peak lime mud-mound, Bare Mountain Quadrangle, Nevada, USA: Ordovician limestone with submarine frost heave structures—a possible response to gas clathrate hydrate evolution. Sediment. Geol. 145 (3–4), 189–213.

Kulm, L.D., Suess, E., 1990. Relationship between carbonate deposits and fluid venting: Oregon accretionary prism. J. Geophys. Res. 95, 8899–8915.

Kvenvolden, K.A., Golan-Bac, M., McDonald, T.J., Pflaum, R.C., Brooks, J., 1989. Hydrocarbon gases in sediment of the Voring Plateau, Norwegian Sea. In: Eldholm, O., Thiede, J., Taylor, E. (Eds.), Proceeding of the ODP, Scientific results Leg 104, Norwegian Sea. ODP, Texas A&M University, College Station, pp. 319–326.

Mazzini, A., Duranti, D., Jonk, R., Parnell, J., Cronin, B.T., Hurst, A., Quine, M., 2003. Palaeo-carbonate seep structures above an oil reservoir, Gryphon Field, Tertiary, North Sea. Geo Mar. Lett. 23 (3–4), 323–339.

Mazzini, A., Ivanov, M.K., Parnell, J., Stadnitskaia, A., Cronin, B.T., Poludetkina, E., Mazurenko, L., van Weering, T.C.E., 2004. Methane-related authigenic carbonates from the Black Sea: geochemical characterisation and relation to seeping fluids. Mar. Geol. 212 (1–4), 153–181.

Mazzini, A., Aloisi, G., Akhmanov, G.G., Parnell, J., Cronin, B., Murphy, P., 2005. Integrated petrographic and geochemical record of hydrocarbon seepage on the Vøring Plateau. Geol. Soc. 162, 815–827.

Mienert, J., Posewang, J., 1999. Evidence of shallow- and deep-water gas hydrate destabilizations in North Atlantic polar continental margin sediments. Geo Mar. Lett. 19 (1–2), 143–149.

Mienert, J., Posewang, J., Baumann, M., 1998. Gas hydrates along the northeastern Atlantic margin: possible hydrate-bound margin instabilities and possible release of methane. In: Henriet, J.P., Mienert, J. (Eds.), Gas Hydrates: Relevance to World Margin Stability and Climate Change. Special Publication — Geological Society of London. Geological Society, pp. 275–292.

Mork, K.A., Blindheim, J., 2000. Variations in the Atlantic inflow to the Nordic Seas, 1955–1996. Deep-sea Res., A, Oceanogr. Res. Pap. 47 (6), 1035–1057.

Naehr, T.H., Rodriguez, N.M., Bohrmann, G., Paull, C.K., Botz, R., 2000. Methane-derived authigenic carbonates associated with gas hydrate decomposition and fluid venting above the Blake Ridge Diapir. In: Paull, C.K., Matsumoto, R., Wallace, P.J., Dillon, W.P. (Eds.), Proc. ODP Scientific Results. College Station, TX (Ocean Drilling Program), pp. 286–300.

Orvik, K.A., Skagseth, O., 2003. Monitoring the Norwegian Atlantic slope current using a single moored current meter. Cont. Shelf Res. 23 (2), 159–176.

Peckmann, J., Reimer, A., Luth, U., Luth, C., Hansen, B.T., Heinicke, C., Hoefs, J., Reitner, J., 2001. Methane-derived carbonates and authigenic pyrite from the northwestern Black Sea. Mar. Geol. 177 (1–2), 129–150.

Posewang, J., Mienert, J., 1999. The enigma of double BSRs: indicators for changes in the hydrate stability field? In: Gardner, J.M., Vogt, P.R. (Eds.), High-latitude gas venting, hydrates and mass wasting. Geomarine Letters. Springer Verlag Kg, pp. 157–163.

Ritger, S., Carson, B., Suess, E., 1987. Methane-derived authigenic carbonates formed by subduction-induced pore-water expulsion along the Oregon/Washington margin. Geol. Soc. Am. Bull. 98, 147–156.

Rokoengen, K., Rise, L., Bryn, P., Frengstad, B., Gustavsen, E., Nygaard, E., Saettem, J., 1995. Upper Cenozoic stratigraphy on the mid-Norwegian continental shelf. Nor. Geol. Tidsskr. 75 (2–3), 88–104.

Savard, M.M., Beauchamp, B., Veizer, J., 1996. Significance of aragonite cements around Cretaceous marine methane seeps. J. Sediment. Res. 66, 430–438.

Skogseid, J., Eldholm, O., 1989. Vøring Plateau continental margin; seismic interpretation, stratigraphy, and vertical movements. In: Eldholm, O., Thiede, J., Taylor, E. (Eds.), Proceeding of the ODP, Scientific results Leg 104, Norwegian Sea. ODP, Texas A&M University, College Station, pp. 993–1030.

Stuevold, L.M., Eldholm, O., 1996. Cenozoic uplift of Fennoscandia inferred from a study of the mid-Norwegian margin. Glob. Planet. Change 12 (1–4), 359–386.

Suess, E., Bohrmann, G., Rickert, D., Kuhs, W., Torres, M., Tréhu, A., Link, P., 2002. Properties and fabric of near-surface hydrates at Hydrate Ridge, Cascadia margin. Fourth Int. Conf. Gas Hydrates, Yokohama, pp. 740–744.

Tchernia, P., 1978. Oceanografie regionale. Ecole Superieure des Tecniques Avancees, Paris. 257 pp. (in French).

Teichert, B.M.A., Gussone, N., Eisenhauer, A., Bohrmann, G., 2005. Clathrites: archives of near-seafloor pore-fluid evolution ($\delta^{44/40}$Ca, δ^{13}C, δ^{18}O) in gas hydrate environments. Geology 33 (3), 213–216.

Vågnes, E., Gabrielsen, R.H., Haremo, P., 1998. Late Cretaceous–Cenozoic intraplate contractional deformation at the Norwegian continental shelf; timing, magnitude and regional implications. Tectonophysics 12, 29–46.

Whiticar, M.J., Faber, E., 1989. Molecular and stable isotope composition of Headspace and total hydrocarbon gases at ODP Leg 104, sites 642, 643, and 644, Vøring Plateau, Norwegian Sea. In: Eldholm, O., Thiede, J., Taylor, E. (Eds.), Proceeding of the ODP, Scientific results Leg 104, Norwegian Sea. ODP, Texas A&M University, College Station, pp. 327–334.